Check for updates

A year-long extended release nanoformulated cabotegravir prodrug

Tanmay A. Kulkarni[2,5], Aditya N. Bade[1,5], Brady Sillman[1], Bhagya Laxmi Dyavar Shetty[1], Melinda S. Wojtkiewicz[1], Nagsen Gautam[2], James R. Hilaire[1], Sruthi Sravanam[1], Adam Szlachetka[1], Benjamin G. Lamberty[1], Brenda M. Morsey[1], Howard S. Fox [1], Yazen Alnouti[2], JoEllyn M. McMillan[1], R. Lee Mosley[1], Jane Meza[3], Paul L. Domanico[4], Tai-Yuen Yue[4], Gary Moore[4], Benson J. Edagwa [1✉] and Howard E. Gendelman [1,2✉]

Long-acting cabotegravir (CAB) extends antiretroviral drug administration from daily to monthly. However, dosing volumes, injection site reactions and health-care oversight are obstacles towards a broad usage. The creation of poloxamer-coated hydrophobic and lipophilic CAB prodrugs with controlled hydrolysis and tissue penetrance can overcome these obstacles. To such ends, fatty acid ester CAB nanocrystal prodrugs with 14, 18 and 22 added carbon chains were encased in biocompatible surfactants named NMCAB, NM2CAB and NM3CAB and tested for drug release, activation, cytotoxicity, antiretroviral activities, pharmacokinetics and biodistribution. Pharmacokinetics studies, performed in mice and rhesus macaques, with the lead 18-carbon ester chain NM2CAB, showed plasma CAB levels above the protein-adjusted 90% inhibitory concentration for up to a year. NM2CAB, compared with NMCAB and NM3CAB, demonstrated a prolonged drug release, plasma circulation time and tissue drug concentrations after a single 45 mg per kg body weight intramuscular injection. These prodrug modifications could substantially improve CAB's effectiveness.

Current antiretroviral drug (ARV) regimens are potent and well-tolerated, enabling the sustained, life-long suppression of human immunodeficiency virus type one (HIV-1) infection[1]. However, viral control is linked to the regimen adherence affected by disease co-morbidity, stigma, behavior, illicit drug-use, and cost[1]. Such limitations were the impetus towards the development of long-acting (LA) injectables[2-6]. In April 2019, ViiV Healthcare submitted a New Drug Application to the US Food and Drug Administration for monthly cabotegravir and rilpivirine (CAB and RPV, respectively) injectables applied in HIV-1 treatments[7]. Although approval was initially denied, the complete response letter received in December 2019[8] focused on Chemistry Manufacturing and Controls, not product safety[8]. Nonetheless, the considerable sustained promise for broad clinical use remains for LA injectables. The 'Antiretroviral Therapy as Long-Acting Suppression' and 'First Long-Acting Injectable Regimen' studies show safety, efficacy and drug tolerability[3,5,6], as do drug implants[9-12]. However, notable limitations in both include injection-site reactions, large injection volumes, frequent dosing, required health-care services and a limited viral tissue reservoir penetrance[4,13,14]. Thus, immediate improvements in LA ARV regimens are needed for use in pre-exposure prophylaxis (PrEP), for HIV-1 transmission control and for maintenance therapy in virologically suppressed patients placed first on other ARV regimens.

To such ends, LA ARV prodrug libraries were created from lipophilic fatty esters to optimize drug release and prodrug hydrolysis rates that result in sustained therapeutic native drug levels in plasma and tissue[14-19]. Despite such improvements, there remains no defined pathway to optimize prodrug hydrolysis rates and other physicochemical features. To this end, we now report the synthesis and physiochemical characterization of variable CAB modified by 14-, 18- and 22-carbon esters (MCAB, M2CAB and M3CAB, respectively) and their respective nanoformulations (NMCAB, NM2CAB and NM3CAB). The lead 18-carbon ester NM2CAB enhanced the human macrophage drug uptake and retention with a sustained protection against the HIV-1 challenge. NM2CAB generated CAB plasma concentrations above the protein-adjusted 90% inhibitory concentration (PA-IC$_{90}$) of 166 ng ml^{-1} for up to one year with detectable lymphoid, mucosal and gut biodistribution (BD) after a single 45 mg per kg body weight parenteral dose with no recorded adverse events in animal models. We posit that optimizing CAB prodrug features could improve native CAB effectiveness and, based on such an extended apparent half-life, could create the potential for a vaccine mimetic.
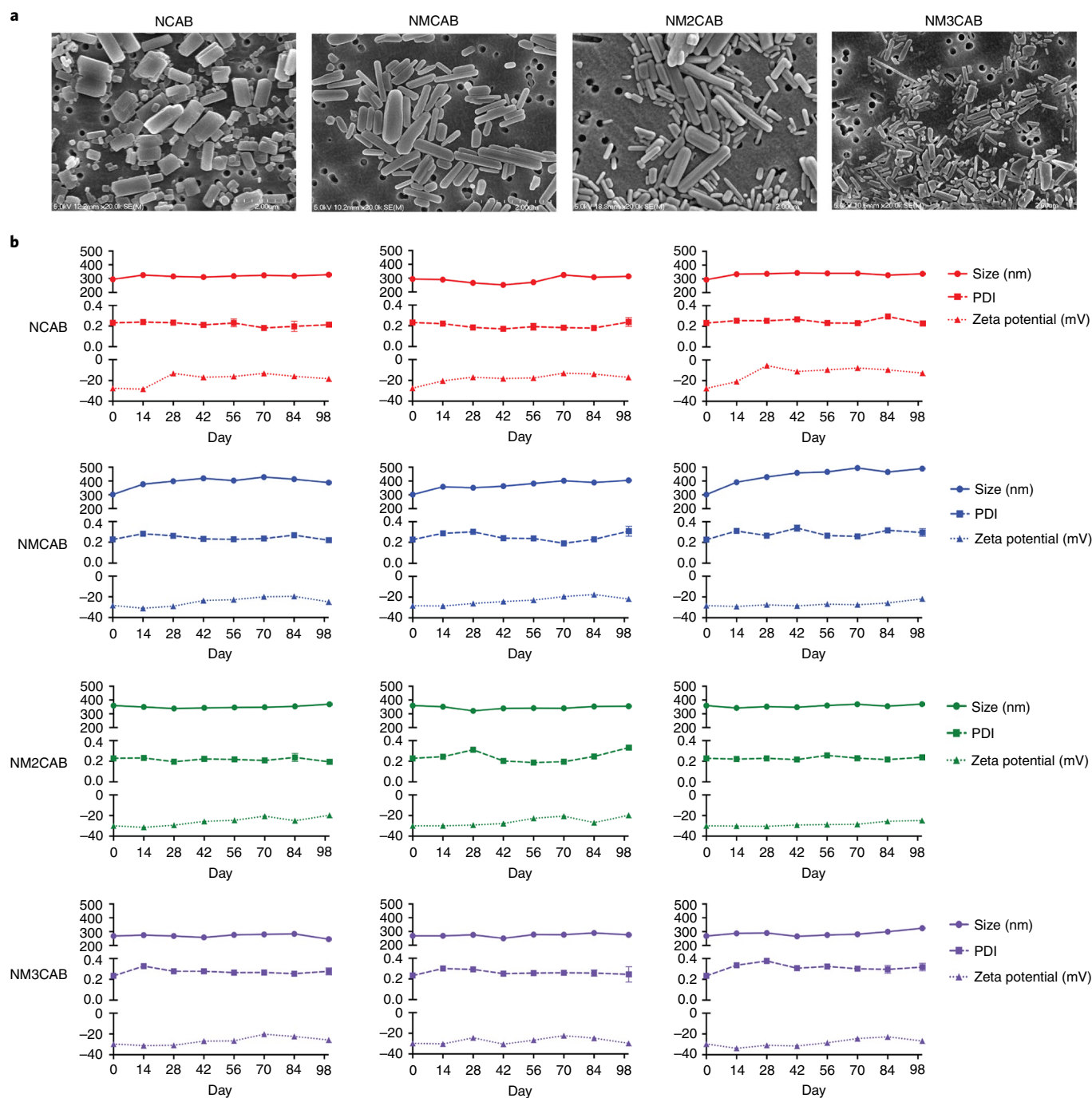
Creation and characterization of CAB prodrugs

CAB was chemically modified by attaching fatty acid esters of variable carbon lengths (C14, C18 and C22) to produce MCAB, M2CAB and M3CAB prodrugs, respectively (Fig. 1a).

Each was characterized by NMR spectroscopy, Fourier transform infrared (FTIR) spectroscopy, electrospray ionization mass spectrometry (MS) and X-ray powder diffraction (XRD) to confirm the chemical structures and purity (Fig. 1b, Supplementary Figs. 1–4 and Supplementary Table 1). There were significant reductions in the aqueous solubility of MCAB ($0.13 \pm 0.03\,\mu g\,ml^{-1}$), M2CAB ($0.10 \pm 0.03\,\mu g\,ml^{-1}$) and M3CAB ($0.04\,\mu g\,ml^{-1}$) compared with that

[1]Department of Pharmacology and Experimental Neuroscience, University of Nebraska Medical Center, Omaha, NE, USA. [2]Department of Pharmaceutical Sciences, University of Nebraska Medical Center, Omaha, NE, USA. [3]Department of Biostatistics, University of Nebraska Medical Center, Omaha, NE, USA. [4]Department of Global Health Sciences, The Clinton Health Access Initiative, Boston, MA, USA. [5]These authors contributed equally: Tanmay A. Kulkarni, Aditya N. Bade. ✉e-mail: benson.edagwa@unmc.edu; hegendel@unmc.edu
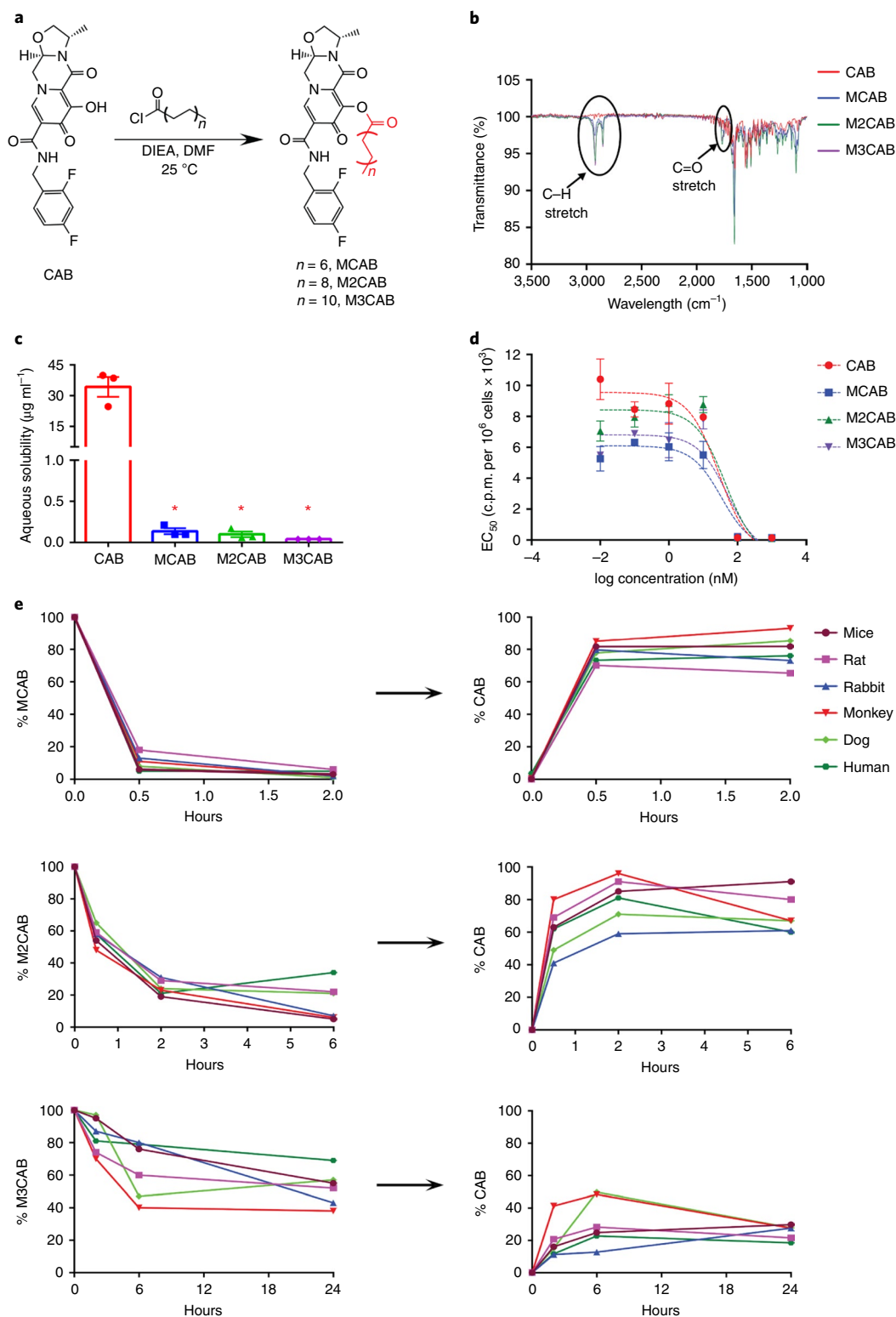
Fig. 1 | Synthesis and characterization of the CAB prodrugs. a, CAB was chemically modified with 14-, 18- and 22-carbon fatty acid chains to develop MCAB, M2CAB, and M3CAB, respectively. **b**, FTIR spectra show the presence of absorption bands at around 2,919 and 1,765 cm^{-1}, which correspond to the C–H stretch in fatty acid methylene groups and the carbonyl stretch, respectively. Data were independently reproduced three times. **c**, Aqueous solubility of CAB and the prodrugs. Data are expressed as the mean ± s.e.m. for $N=3$ (CAB), 3 (NMCAB), 3 (NM2CAB) and 3 (NM3CAB) biologically independent samples. A t-test (two-tailed) with Welch's correction was used to compare the solubility between CAB and individual prodrugs. *$P < 0.05$. **d**, Antiviral activity (EC$_{50}$) was determined in the MDM over a range of concentrations (0.01–1,000 nM) by measuring the HIV-1 RT activity after challenge with HIV-1$_{ADA}$ at a multiplicity of infection of 0.1. Data are expressed as the mean ± s.e.m. for $N=3$ biological replicates. **e**, Plasma cleavage kinetics. The bioconversion of prodrugs (left) into active CAB (right) in the plasma of various species (mice, rat, rabbit, monkey, dog and human) was assessed. Experiments were repeated independently twice with equivalent results. DIEA, N,N-diisopropylethylamine; DMF, dimethylformamide.

Fig. 2 | Synthesis and characterization of nanoformulations of CAB and prodrugs. a, Morphological assessment of NCAB, NMCAB, NM2CAB and NM3CAB by SEM. Data were independently reproduced three times. **b**, The stabilities of CAB and the prodrug nanoformulations were evaluated over 98 days after the manufacture at room temperature (left), 4 °C (centre) and 37 °C (right), as determined by size, PDI and zeta potential. Data are expressed as the mean ± s.e.m. for $N = 3$ biological replicates.

of CAB ($34.31 \pm 4.8 \, \mu g \, ml^{-1}$) were recorded (Fig. 1c). The log P values (for partition coefficient P) for MCAB, M2CAB and M3CAB were 4.56, 4.89 and 5.12, respectively, compared with 0.16 for CAB (Supplementary Table 1). These results confirmed the enhanced prodrug hydrophobicity and lipophilicity.

Pharmacologically inactive prodrugs require enzymatic or hydrolytic activation in physiological conditions for active drug bioconversion[20,21]. Therefore, the hydrolysis kinetics of MCAB, M2CAB and M3CAB and subsequent CAB formation were evaluated in mouse, rat, rabbit, monkey, dog and human plasma and demonstrated a >85%

cleavage of MCAB in 30 minutes. M2CAB showed an average of 75 and 80% cleavage within two and six hours, respectively. M3CAB showed 50% prodrug cleavage after 24 hours (Fig. 1e). The differences in prodrug hydrolysis paralleled divergent species-specific plasma esterase activities[22]. Next, the half-maximum effective concentrations (EC_{50}) of MCAB, M2CAB and M3CAB were tested. HIV-1 reverse transcriptase (RT) activities in the culture medium of monocyte-derived macrophages (MDMs) infected with HIV-1 strain ADA (HIV-1$_{ADA}$) demonstrated comparable EC_{50} values, indicating that the modifications did not affect drug antiviral activities (Fig. 1d).

Manufacturing and long-term formulation stability

Scalable nanocrystal manufacture techniques[23,24] were employed to generate the nanoformulations of NCAB, NMCAB, NM2CAB and NM3CAB by high-pressure homogenization. Drug loading for CAB and M2CAB was >80% with <1% of uncoated prodrug in the NM2CAB nanocrystals, using poloxamer 407 (P407) as the stabilizer in water (Supplementary Table 2). Scanning electron microscopy (SEM) images showed uniform rod-shaped nanoparticle morphologies (Fig. 2a). Nanoparticle sizes, polydispersity indices (PDI) and zeta potentials were determined as measures of stability by dynamic light scattering (at room temperature, 4 °C and 37 °C (Fig. 2b). Particle sizes and PDIs remained narrow over 98 days, which indicates minimal aggregation. Zeta potentials of −25 to −35 mV indicated a high particle stability through electrostatic repulsion. All the formulations remained stable for up to 98 days, which signifies that the nanosuspensions maintain their integrity under a range of storage conditions, reflective of the need in resource-limited settings (Fig. 2b). Reproducibility was confirmed in 11 separate NM2CAB batches (Supplementary Table 3). Nanoparticle sizes varied from 243 ± 2 to 378 ± 1 nm with a narrow PDI (0.18 to 0.33).

Nanoformulation effects on the prodrug antiretroviral activity (EC_{50}) were determined in MDM (Supplementary Fig. 5). EC_{50} values were increased compared with those of the non-nanoformulated drug or prodrugs. The required nanoparticle dissolutions, prior to cleavage of the prodrugs, could account for the increased EC_{50} values and were comparable for those of NCAB (39.83 nM), NMCAB (89.67 nM) and NM2CAB (37.02 nM). However, the EC_{50} value for NM3CAB increased ($\sim 1.78 \times 10^6$ nM), which could be linked to a slower prodrug conversion to active CAB (Fig. 1e). Cellular vitality was assessed in MDM using the 3-(4,5-dimethylthiazol-2-yl)-2,5-diphenyltetrazolium bromide (MTT) assay (Supplementary Fig. 6). No formulation-induced cytotoxicity was seen at 10–400 μM drug or prodrug concentrations.

MDM uptake, retention, release and antiretroviral efficacy

Macrophage phagocytic and tissue migratory functions enable the cell to be used as drug carriers and depots[14,25–27]. Therefore, laboratory macrophage modelling was used to assess the uptake, retention, release and antiretroviral activities of nanoformulated ARV prodrugs[14,16–19]. Formulation uptake was assessed in MDM by measuring the drug and prodrug levels after 100 μM treatment with NCAB, NMCAB, NM2CAB or NM3CAB over 24 hours (Fig. 3a). Intracellular prodrug levels for NMCAB, NM2CAB and NM3CAB were 61.69 ± 0.78, 84.07 ± 5.82 and 73.34 ± 13.59 nmol per 10^6 cells, respectively, at 24 hours; and intracellular CAB levels were 0.58 ± 0.11, 12.31 ± 0.46, 17.79 ± 2.92, and 7.97 ± 1.76 nmol per 10^6 cells for NCAB, NMCAB, NM2CAB and NM3CAB, respectively (Fig. 3a). After treatment with 100 μM of each nanoformulation for eight hours, we evaluated the ability of macrophages to retain intracellular drugs and prodrugs over a period of 30 days (Fig. 3b). Intracellular prodrug levels were sustained for 30 days at 0.41 ± 0.09,

14.21 ± 2.28 and 26.70 ± 3.29 nmol per 10^6 cells for NMCAB, NM2CAB and NM3CAB, respectively (Fig. 3b). Similarly, intracellular CAB levels formed from prodrug cleavage for NM2CAB and NM3CAB were 1.71 ± 0.35 and 2.05 ± 0.10 nmol per 10^6 cells at day 30. NMCAB treatment showed CAB levels at the detection limit at day 25. CAB levels fell below the limit of quantitation after one day of NCAB treatment (Fig. 3b). CAB released from these cells into culture medium was also measured. NM2CAB provided the most sustained CAB release with medium drug concentrations of 1.98 ± 0.18 nmol ml^{-1} at day 10 and 1.0 ± 0.10 nmol ml^{-1} at day 30. CAB release from the NMCAB-treated cells was rapid with concentrations of 16.29 ± 0.84 nmol ml^{-1} at day 10 and 3.19 ± 1.46 nmol ml^{-1} at day 30. CAB was not detected in the culture medium with NCAB and NM3CAB treatments after five and ten days, respectively (Fig. 3c). Prodrugs were not detected in the culture medium for any of the treatments. Transmission electron microscopy (TEM) images of MDM confirmed the presence of prodrug nanoformulations (NM2CAB and NM3CAB) in cytoplasmic vesicles, which further signifies a macrophage drug depot (Fig. 3d). To determine whether a sustained drug retention in MDM would protect against HIV-1 infection, we challenged cells with HIV-1$_{ADA}$ for up to 30 days after treatment with 100 μM NCAB, NMCAB or NM2CAB. NM3CAB was not selected for this study as it did not show protection at the desired EC_{50} value (Supplementary Fig. 5). NM2CAB treatment suppressed the HIV-1 RT activity (Fig. 3e) as was confirmed by the absence of HIV-1 p24 expression up to day 30 (Fig. 3f). In contrast, complete viral breakthrough occurred at day 1 after NCAB and day 20 after NMCAB treatment. NM2CAB provided a 'best' protection against HIV-1 challenge. In addition, 10, 50 or 100 μM NM2CAB treatment induced sustained antiretroviral activity (Fig. 3g,h). Complete viral suppression was observed with 50 and 100 μM NM2CAB treatments, whereas 10 μM treatment provided 57% protection after 30 days (Fig. 3g); the results were validated by HIV-1 p24 expression (Fig. 3h).

## Year-long plasma CAB levels after a single NM2CAB injection

To assess the pharmacokinetic (PK) and BD profiles, female NSG (non-obese diabetic scid gamma) mice were injected intramuscularly (IM) with a single dose of 45 mg per kg body weight CAB equivalents of NCAB, NMCAB or NM2CAB. NCAB reflects the US Food and Drug Administration filed CAB LA and thus was used as a control (Supplementary Fig. 7). At day 1 after NCAB treatment, higher plasma CAB concentrations were detected compared with those of both NMCAB and NM2CAB. However, NCAB showed a faster decay compared with that of NM2CAB (Fig. 4). For NCAB treatment, plasma CAB concentrations were above $4 \times$ PA-IC$_{90}$ (664 ng ml^{-1}) up to day 35 (792.7 ng ml^{-1}), and then rapidly declined to below PA-IC$_{90}$ (166 ng ml^{-1}) by day 49 (75 ng ml^{-1}). At day 126, the CAB values were below the limit of detection (0.5 ng ml^{-1}). NMCAB treatment showed a slower CAB decay, and the CAB levels were

Fig. 3 | In vitro characterization. a,b, Cellular uptake (**a**) and retention (**b**) of the drug and each prodrug in MDM was assessed. **c**, In parallel, CAB released into the culture medium was measured. For the uptake study, a one-way analysis of variance (ANOVA) followed by Tukey's post hoc test was used to compare the CAB levels among four treatment groups (red, ##$P < 0.01$, ***$P < 0.001$, $$$$P < 0.0001$ compared with NCAB) and the prodrug levels among three treatment groups (blue, @$P < 0.05$ compared NMCAB). For the retention study, a one-way ANOVA followed by Tukey post hoc test was used to compare the CAB levels among four treatment groups (red, $$$$P < 0.0001$, ####$P < 0.0001$ compared with NCAB) and prodrug levels among three treatment groups (blue, @@$P < 0.01$, ^^^$P < 0.001$ compared with NMCAB, and green, ^^$P < 0.01$ compared with NM2CAB). For the release study, a one-way ANOVA followed by Tukey's post hoc test was used to compare CAB levels among four treatment groups (red, *$P < 0.05$). For all assays, data are expressed as mean ± s.e.m., $N = 3$ biological replicates. **d**, TEM images of MDM treated with each nanoformulation and of the untreated control. Red arrowheads indicate nanocrystals present in the cytoplasm. Scale bars, 2 μm. Data were independently reproduced three times. **e,f**, Antiretroviral activity. Infection was determined by measuring the HIV-1 RT activity in culture medium (**e**) and HIV-1 p24 antigen immunocytochemistry (**f**). **g,h**, The antiretroviral activities of NM2CAB was determined by measures of HIV-1 RT activity in culture supernatants (**g**) and by cell-associated HIV-1p24 antigens by immunonocytochemistry (**h**) **e,g**, HIV-1 RT activity is expressed as mean ± s.e.m., $N = 4$ biological replicates. **f,h**, Each experiment was repeated independently three times with equivalent results.

maintained above $4 \times$ PA-IC$_{90}$ up to day 91 (673.8 ng ml^{-1}) and above the PA-IC$_{90}$ at 186.7 ng ml^{-1} at day 168. At day 364 after NMCAB treatment, the CAB levels were 8.5 ng ml^{-1}. NM2CAB demonstrated

a slower plasma CAB decay compared with those of both NCAB and NMCAB for the entire study, and maintained sustained plasma CAB levels above the $4 \times$ PA-IC$_{90}$ at 702.0 ng ml^{-1} at day 231 and
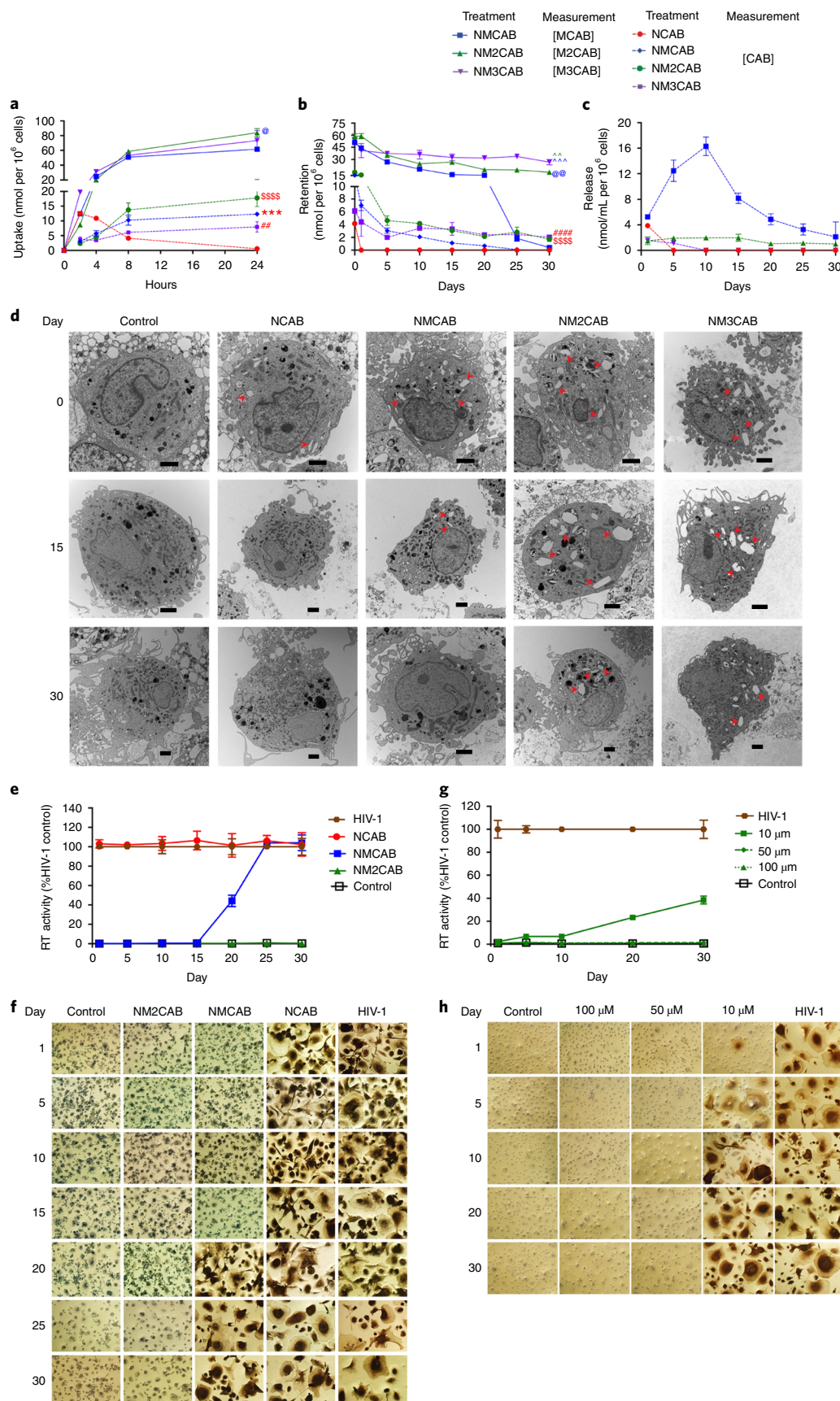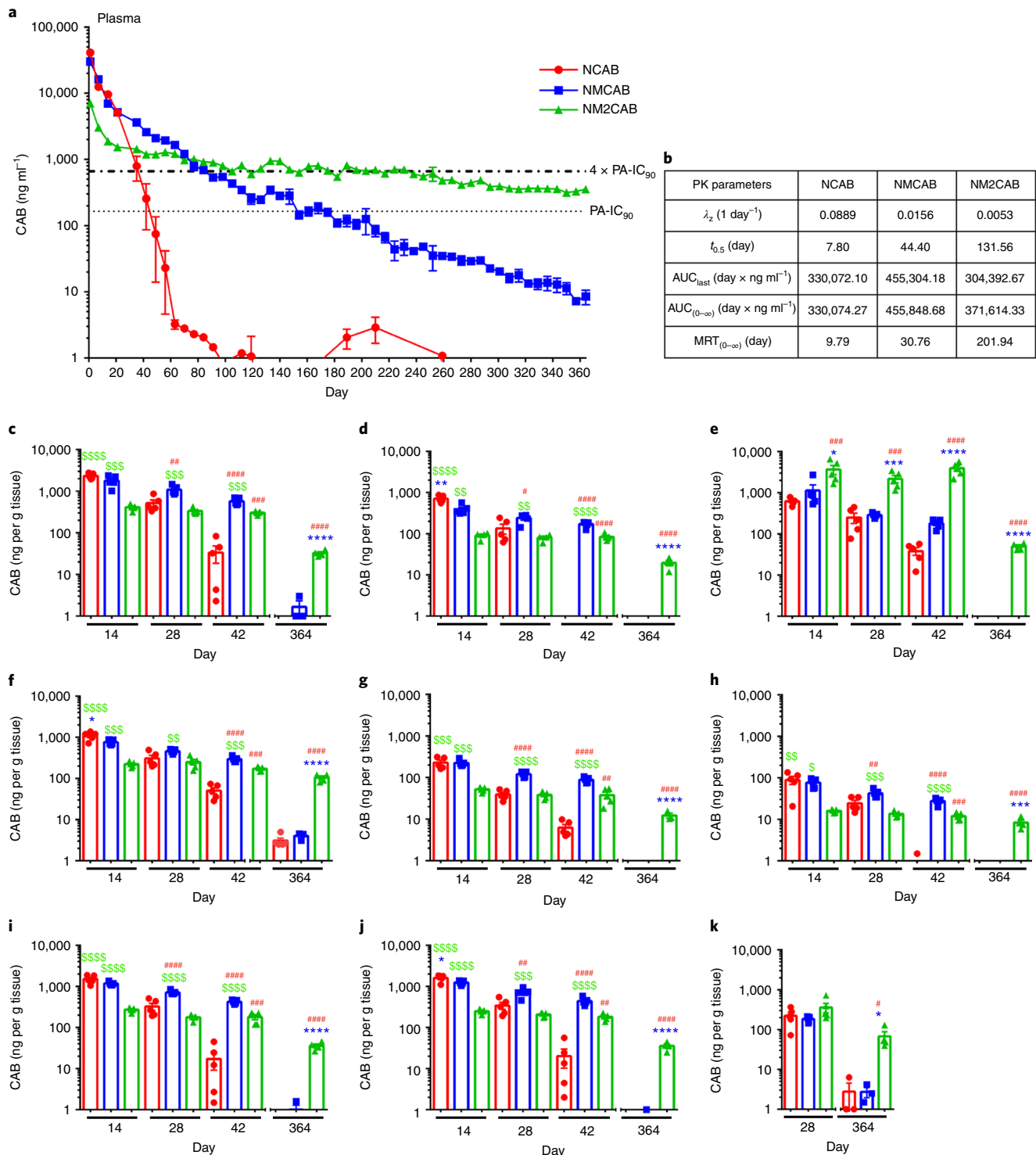
Fig. 4 | CAB levels in plasma and tissues. a, Plasma drug levels in NSG mice. The bold dashed line indicates the plasma CAB $4 \times$ PA-IC$_{90}$ (664 ng ml^{-1}), and bottom dotted line shows the plasma CAB $1 \times$ PA-IC$_{90}$ (166 ng ml^{-1}). Data are expressed as mean $\pm$ s.e.m. Study was initiated with $N = 5$ animals per group. Owing to loss of animals by natural causes during study period, animals at day 364 were $N = 5$ (NCAB), $N = 3$ (NMCAB) and $N = 4$ (NM2CAB). **b**, Plasma PK parameters for CAB were determined using non-compartmental analyses. λ_z, individual estimate of the terminal elimination rate constant; AUC$_{0-\infty}$, area under the plasma concentration time curve (AUC) from 0 hours to infinity; AUC$_{last}$, AUC from 0 hours to last time point; MRT$_{0-\infty}$, MRT from 0 hours to infinity. **c**–**k**, Tissue BD of CAB was assessed at days 14, 28, 42 and 364 in vaginal tissue (**c**), rectal tissue (**d**), spleen (**e**), liver (**f**), gut (**g**), brain (**h**), kidney (**i**), lung (**j**) and lymph node anatomical associated tissues (**k**). Drug levels in the lymph nodes (**k**) were determined in anatomical regions associated with lymph nodes only at days 28 and 364, due to their immature state in immunodeficient NSG mice. **c**–**k**, Data are expressed as mean $\pm$ s.e.m. For days 14, 28 and 42 groups, $N = 5$ animals per group, and for day 364, $N = 5$ (NCAB), $N = 3$ (NMCAB) and $N = 4$ (NM2CAB) animals through natural causes. A one-way ANOVA followed by Tukey's post hoc test was used to compare the drug levels in tissues among the three treatments (red, $^\#P < 0.05$, $^{\#\#}P < 0.01$, $^{\#\#\#}P < 0.001$, $^{\#\#\#\#}P < 0.0001$ compared with NCAB; blue, $^*P < 0.05$, $^{**}P < 0.01$, $^{***}P < 0.001$, $^{****}P < 0.0001$ compared with NMCAB; green, $^\$P < 0.05$, $^{\$\$}P < 0.01$, $^{\$\$\$}P < 0.001$, $^{\$\$\$\$}P < 0.0001$ compared with NM2CAB).

above the PA-IC$_{90}$ at 354 ng ml^{-1} at day 364. PK parameters were determined using non-compartmental analysis for all treatment groups (Fig. 4b). The apparent CAB half-life ($t_{0.5}$) after NM2CAB treatment (131 days) was 17- and 3-fold longer than those of NCAB (7 days) and NMCAB (44 days), respectively. Similarly, the CAB mean residence time (MRT) of NM2CAB (201 days) was 21-fold longer than that of NCAB (9 days) and 7-fold longer than that of NMCAB (30 days). NM2CAB elicited higher CAB tissue levels than the NMCAB and NCAB treatments (Fig. 4c–k). At day 28, the CAB tissue levels were comparable between NCAB and NM2CAB. However, by day 42, the CAB tissue levels after NCAB treatment were lower than those observed for NM2CAB (vagina, spleen, gut, liver, lymph node, kidney, lung, rectum and brain). CAB levels in tissues, up to day 42 after NMCAB treatment, were substantially higher than those of NCAB and NM2CAB. However, at day 364, CAB concentrations were readily found in tissues in the NM2CAB-treated group. CAB levels were 32.5, 19.6, 49.7 and 67.6 ng per g tissue in the vagina, rectum, spleen and lymph nodes, and 104.4, 12.3, 8.3, 36.0 and 35.5 ng per g tissue in the liver, gut, brain, kidney and lung (Fig. 4c–k). MCAB and M2CAB prodrug concentrations were also quantified in blood and tissues (Fig. 5). At day 1 after injection, the MCAB and M2CAB concentrations in blood were 22 and 31.3 ng ml^{-1}, respectively, and rapidly declined below the limit of detection thereafter (Fig. 5i). All the screened tissues were prodrug depots (Fig. 5a–h). Notably, the MCAB levels were substantially lower than the M2CAB levels at days 14, 28 and 42, and were undetectable by day 364. For NM2CAB at day 364, the prodrug levels were 2,973.3, 958.4, 38.5, 50.3, 4.2 and 18,710.1 ng per g tissue in the spleen, liver, lung, brain, kidney and lymph nodes, respectively. Next, a single IM injection of NM3CAB (45 mg per kg body weight CAB equivalents) in female NSG mice generated lower levels of plasma CAB (2,248 ng ml^{-1}) at day 1 compared with 41,237.6, 30,148.9 and 7,076.1 ng ml^{-1} for NCAB, NMCAB and NM2CAB, respectively (Supplementary Fig. 8). Plasma CAB levels were around the PA-IC$_{90}$ level (233.2 ng ml^{-1}) within 28 days after treatment. In addition, CAB levels in the tissues (spleen, liver, brain, gut and lymph nodes) reflected low plasma CAB concentrations at day 28 (Supplementary Fig. 8). The slower hydrolysis of M3CAB was validated in BALB/cJ mice (Supplementary Fig. 9). Similar to the PK results in NSG mice, NM3CAB treatment generated low levels of plasma CAB that fell below the PA-IC$_{90}$ by 28 days with values of 98.8 ng ml^{-1}. These data confirmed an impeded hydrolysis of M3CAB to CAB. Therefore, as our objective is to develop a formulation with a six months or longer dosing interval, the NM3CAB treatment group was terminated from further evaluation.

Superior PK and BD profiles of NM2CAB among all the formulations were confirmed in BALB/cJ mice. Normal mice were used to validate the results from immunodeficient NSG mice. The PK and BD assessments in plasma and tissues for NM2CAB paralleled those in NSG mice (Supplementary Fig. 10). Plasma CAB concentrations of 170.8 ng ml^{-1} were above the PA-IC$_{90}$ at day 231. In contrast, CAB plasma levels after NCAB treatment fell below the PA-IC$_{90}$ to 12.3 ng ml^{-1} at day 28. To validate the results seen in mice, rhesus macaques (RMs) were injected IM with a single dose of 45 mg per kg body weight CAB equivalents of NM2CAB (Fig. 6). Plasma CAB

and M2CAB prodrug levels were measured up to day 365. Similar to the results in mice, NM2CAB treatment provided slow plasma CAB decay kinetics, which maintained plasma CAB concentrations for up to 364 days. CAB levels were measured at an average of 66.9 ng ml^{-1}. As observed in mice, plasma M2CAB concentrations were lower throughout the study compared with the CAB levels (Fig. 6a). At day 204 after NM2CAB administration, CAB concentrations in rectal, lymph node and adipose tissues were 10.1, 21.9 and 29.5 ng per g tissue, respectively (Fig. 6b). M2CAB was present at higher levels in lymph node and adipose tissues (33.3 and 233.2 ng per g tissue) with lower levels (1.7 ng per g tissue) in rectal tissue (Fig. 6c). Statistical analysis determined that the assessment in macrophages directly correlated with PK measurements (Supplementary Table 4).

Toxicity assessments

Toxicity was assessed in mice and RMs after NM2CAB treatment. For NSG mice, animal weights were recorded weekly for one year; at the study conclusion (day 364), plasma and tissues were collected for metabolic profiles and histopathology, respectively (Supplementary Fig. 11). Controls were age-matched untreated mice. No differences in weights were observed between the control and treatment groups (Supplementary Fig. 11a). Comprehensive serum chemistry profiles were quantified; no notable differences were noted between the controls and NM2CAB-treated groups (Supplementary Fig. 11b), which indicates that NM2CAB did not adversely affect the functions of systemic organs. Haematoxylin and eosin-stained tissue sections, examined by a certified pathologist, revealed no abnormal pathology in NM2CAB-treated animals (Supplementary Fig. 11c). For the assessment in RMs, weights were recorded, and complete blood counts and metabolic profiles were assessed for up to 365 days after NM2CAB dosing (Fig. 6d,e). No changes in the weights of any animals were observed (Supplementary Fig. 12). An initial mild redness observed at the site of injection resolved by day 3 in all animals. Total white cell, neutrophil, lymphocyte and monocyte counts were unchanged during the study period (Fig. 6d). At day 1 after injection, increased neutrophil counts were observed, which then resolved to normal within 2 weeks for all animals. Such a change could be related to the injection itself and not be drug-associated[28]. Liver and kidney metabolic profiles were unchanged in all animals after treatment (Fig. 6e). Overall, no adverse events were observed after NM2CAB administration.

ARV prodrug drug–drug interactions

We evaluated the potential of drug–drug interactions between NM2CAB and a best-performing RPV prodrug nanoformulation (NM3RPV). RPV was chosen along with CAB based on the current clinical development of CAB LA and RPV LA formulations for combination treatment[3–6]. NM3RPV is a LA prodrug formulation of RPV developed by our laboratory[16]. BALB/cJ male mice were treated IM with a single dose of NM2CAB alone, NM3RPV alone or co-administration of NM2CAB and NM3RPV. No differences in plasma CAB and RPV concentrations were observed between animals treated with single or combined drug formulations (Supplementary Fig. 13).

Fig. 5 | Prodrug measurements. Tissue and blood concentrations of prodrugs (MCAB or M2CAB) were determined at 14, 28, 42 and 364 days after a single IM injection of NMCAB or NM2CAB. **a–h**, Prodrug levels were measured in the spleen (**a**), liver (**b**), gut (**c**), lung (**d**), brain (**e**), rectal tissue (**f**), kidneys (**g**), lymph node anatomical associated tissues (**h**) and blood (**i**). Prodrug levels in the lymph nodes were determined in anatomical regions associated with the lymph nodes only at days 28 and 364, due to their immature state in immunodeficient NSG mice. **a–h**, Data are expressed as mean ± s.e.m. For days 14, 28 and 42 groups, animal numbers in each group were $N = 5$, and for the day 364 groups, animal numbers were $N = 3$ (NMCAB) and $N = 4$ (NM2CAB). A t-test (two-tailed) with Welch's correction was used to compare the prodrug levels in tissues at the respective time points ($*P < 0.05$, $**P < 0.01$, $***P < 0.001$, $****P < 0.0001$). **i**, Data are expressed as mean ± s.e.m. The study was initiated with $N = 5$ animals in each group (NCAB, NMCAB or NM2CAB). Owing to the loss of animals by natural causes during the study period, by day 364 post-treatment there were $N = 5$ (NCAB), $N = 3$ (NMCAB) and $N = 4$ (NM2CAB) animals.

Formulation scalability

Given the need for bench-to-bedside translation, we examined NM2CAB's scalability. First, we recrystallized then produced NM2CAB at high prodrug concentrations. Recrystallization provides purity control and is broadly used by the pharmaceutical industry[29]. For NM2CAB recrystallization, the solvents tested were
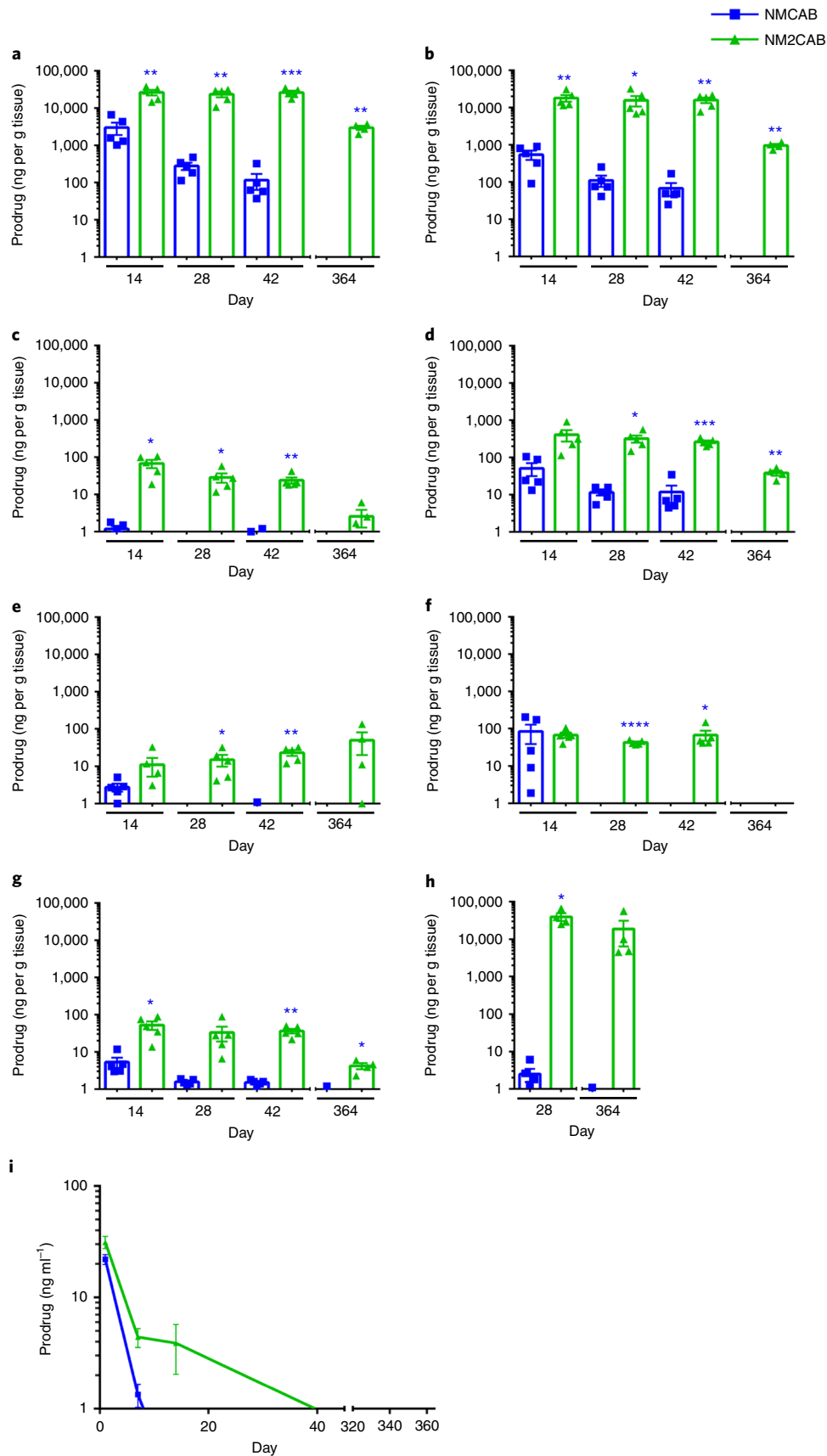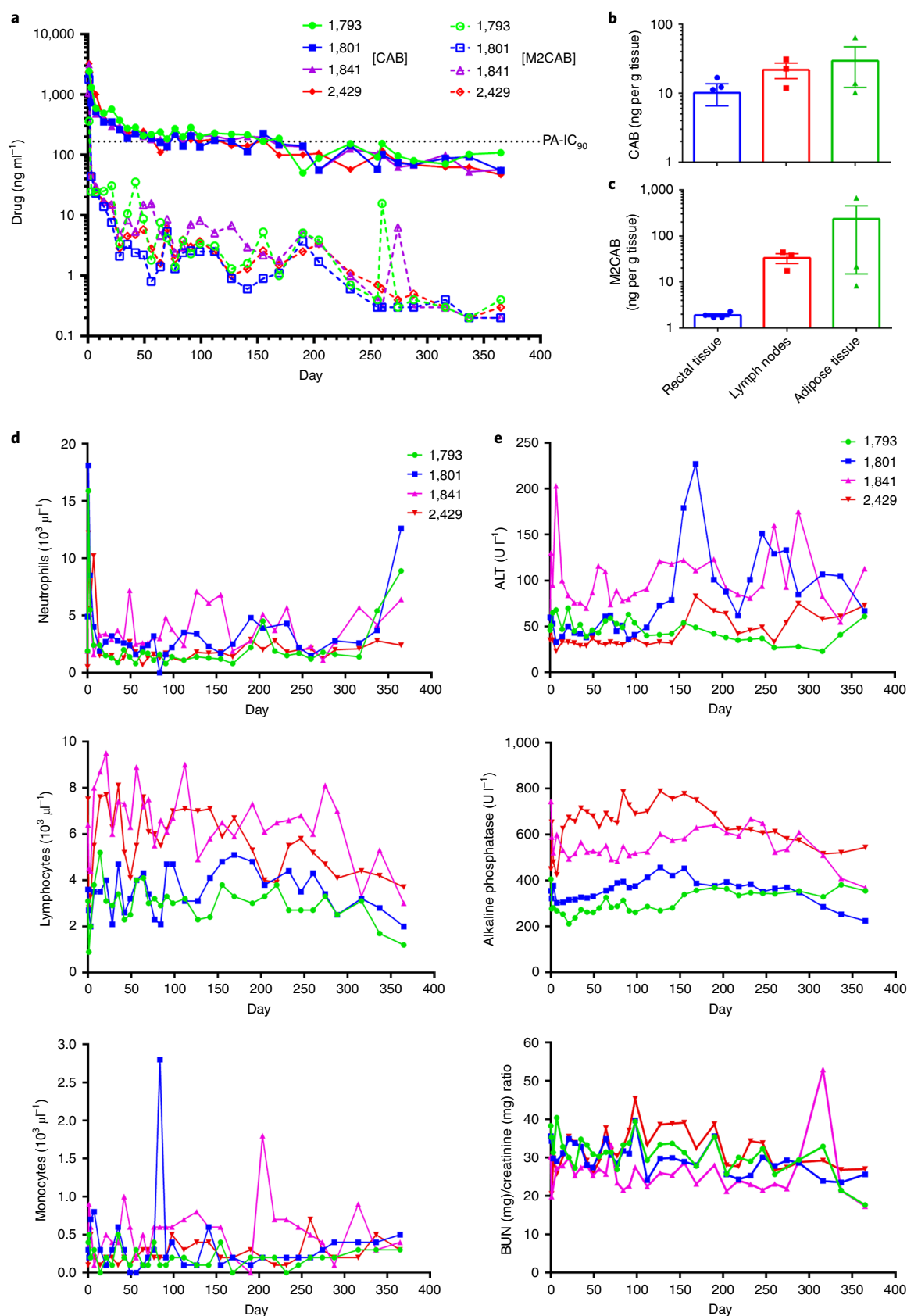
Fig. 6 | PK, BD and toxicological assessments in RMs. Four RMs were administered a 45 mg per kg body weight CAB-equivalent dose of NM2CAB by a single IM injection. **a**, Plasma samples were collected, and CAB and M2CAB levels were determined up to day 365. **b,c**, Rectal, lymph node and adipose tissue biopsies were collected at day 204 after drug administration and assayed for CAB (**b**) and M2CAB (**c**) concentrations. **d,e**, Systemic adverse reactions were evaluated by measuring haematological (**d**) and metabolic (**e**) profiles. Plasma drug and prodrug concentrations as well as haematological and metabolic profile parameters are shown for individual animals. Tissue drug concentrations are expressed as mean ± s.e.m.; $N = 4$ animals. BUN, blood urea nitrogen.

acetonitrile (ACN), methyltetrahydrofuran, cyclopentyl methyl ether (CPME) and toluene. Recovery yields, melting points and purity were determined (Supplementary Table 5). M2CAB yields were highest for ACN (70%) and CPME (85%). Recovery was temperature and solubility dependent. The melting point was narrow after recrystallization for all the solvents. A modest increase in the melting point was observed for ACN solids (123–125 °C) compared with that of the original sample (116–122 °C). The purity profiles of M2CAB before and after recrystallization from ACN and CPME were equivalent (Supplementary Table 5). The XRD assessment of the physical appearances of the solids from ACN and CPME were similar to the those of the original M2CAB (Supplementary Fig. 14). Next, the manufacturing scheme for a scale-up production of NM2CAB at high concentrations was evaluated. Stable NM2CAB was manufactured at a 400 mg ml^{-1} drug concentration under good laboratory practices. Thus, <1 ml of NM2CAB injection volume would be required in patients when extrapolated from current dosing[30].

Discussion

LA ARVs suppress viral replication equally to oral medicines while affecting regimen adherence[4–6,31–33]. The development of LA slow effective release antiretroviral therapy (LASER ART) formulations by our laboratories has given additional promise to the first phase of LA regimens[34]. Here, a single injection of NM2CAB generated substantial improvements in drug PK, reflected by sustained plasma drug concentrations and tissue BD compared with those of NCAB, NMCAB and NM3CAB. NM2CAB provided an extended plasma CAB decay in mice and RMs while maintaining drug levels above the PA-IC$_{90}$ of 166 ng ml^{-1} for one year after a single injection. In all, an approximate 20-fold improvement in PK parameters was seen compared with those of the first-generation CAB LA. The variability in plasma CAB concentrations among the tested strains and species could be a result of differences in body fat distribution, muscle mass, physical activity and carboxylesterases enzymes required for prodrug hydrolysis[22,35,36]. CAB LA was studied extensively in RMs. These studies demonstrated that CAB LA provided a high degree of protection against vaginal, rectal, parenteral and penile challenges with simian-HIV strains, which affirms its future use as PrEP for people at high risk for sexual HIV-1 exposure and for intravenous drug users[37,38]. Plasma levels above $3 \times$ PA-IC$_{90}$ provided 100% protection, and concentrations above the PA-IC$_{90}$ provided 97% protection against viral challenge. Here, NM2CAB administration generated plasma CAB concentrations above PA-IC$_{90}$ for up to a year, which signifies its potential use for PrEP. Moreover, there are several advantages of NM2CAB over the investigational CAB LA. First, the manufacture of NM2CAB at a concentration of 400 mg ml^{-1}, which is twice the 200 mg ml^{-1} for CAB LA. Second, NM2CAB would require <1 ml of injection volume for a yearly administration rather than the 2 ml injection volume of CAB LA for a monthly dosing. Thus, NM2CAB can overcome major obstacles of CAB LA: dosing volume, administration intervals and injection site reactions.

The discoveries made in this report demonstrate a 'sweet spot' in prodrug product profiles that enables an important extension in CAB's apparent half-life, safety of administration and ease of manufacture for immediate global PrEP. The innovative molecular design of the prodrug not only provided favourable physicochemical properties, but also resulted in a crystalline and thermally stable compound that facilitates its successful manufacture. Importantly, similar approaches may improve the PK and targeting properties of medicines used to treat a spectrum of infectious, inflammatory, metabolic and/or degenerative disorders[39].

Nonetheless, CAB LA formulations can meet the challenge of therapeutic regimen adherence in broad patient groups, which include children, adolescents and pregnant and postpartum women[4,37,38]. Although Phase 2 and Phase 3 LA ARV clinical trials are encouraging[5,6,13,40,41], limitations are acknowledged, which include requirements for an oral lead in for safety. Moreover, a prolonged pharmacologic tail after discontinuation could result in drug-resistant viral strains as reported for RPV LA[42]. The lack of activity against major co-infections, such as hepatitis B virus[43], and potential drug–drug interactions are other considerations. For example, the combined use of CAB and rifampin could reduce CAB exposure. Individuals who receive such a once-a-year CAB and are diagnosed with tuberculosis would be cautioned against the use of rifampin. Here, rifabutin would be an alternative[44,45].

Taken together, CAB prodrugs chemically modified with 14, 18 or 22 carbon chain esters encased into surfactant-coated nanoformulations were created. Evaluations of prodrug hydrolysis and PK profiles demonstrated that NM2CAB produced a 'once-a-year' injectable profile. Particularly, in the absence of protective vaccines against HIV-1[46,47], effective LA ART not only are the best approaches for PrEP[47], but also could serve as a vaccine mimetic if dosing intervals are extended to yearly or longer. Moreover, CAB's activities against HIV-2 provide a real potential for dual treatment[48,49]. Altogether, we conclude that a major extension of the dosing interval could allow NM2CAB to be developed as a vaccine mimetic.

Online content

Any methods, additional references, Nature Research reporting summaries, source data, extended data, supplementary information, acknowledgements, peer review information; details of author contributions and competing interests; and statements of data and code availability are available at https://doi.org/10.1038/s41563-020-0674-z.

References

1. Fauci, A. S., Redfield, R. R., Sigounas, G., Weahkee, M. D. & Giroir, B. P. Ending the HIV epidemic: a plan for the United States. *J. Am. Med. Assoc.* **321**, 844–845 (2019).
2. Gendelman, H. E., McMillan, J., Bade, A. N., Edagwa, B. & Kevadiya, B. D. The promise of long-acting antiretroviral therapies: from need to manufacture. *Trends Microbiol.* **27**, 593–606 (2019).
3. Currier, J. S. Monthly injectable antiretroviral therapy—version 1.0 of a new treatment approach. *N. Engl. J. Med.* **382**, 1164–1165 (2020).
4. Margolis, D. A. et al. Long-acting intramuscular cabotegravir and rilpivirine in adults with HIV-1 infection (LATTE-2): 96-week results of a randomised, open-label, phase 2b, non-inferiority trial. *Lancet* **390**, 1499–1510 (2017).
5. Orkin, C. et al. Long-acting cabotegravir and rilpivirine after oral induction for HIV-1 Infection. *N. Engl. J. Med.* **382**, 1124–1135 (2010).
6. Swindells, S. et al. Long-acting cabotegravir and rilpivirine for maintenance of HIV-1 suppression. *N. Engl. J. Med.* **382**, 1112–1123 (2020).
7. ViiV Healthcare submits new drug application to US FDA for the first monthly, injectable, two-drug regimen of cabotegravir and rilpivirine for treatment of HIV (ViiV Healthcare, 2019); https://viivhealthcare.com/en-gb/media/press-releases/2019/april/viiv-healthcare-submits-new-drug-application-to-us-fda-for-the-first-monthly-injectable-two-drug-regimen-of-cabotegravir-and-rilpivirine-for-treatment-of-hiv/
8. ViiV Healthcare receives complete response letter from US FDA for use of investigational cabotegravir and rilpivirine long-acting regimen in the treatment of HIV (ViiV Healthcare, 2019); https://viivhealthcare.com/en-gb/media/press-releases/2019/december/complete-response-letter-from-us-fda/
9. Kovarova, M. et al. Ultra-long-acting removable drug delivery system for HIV treatment and prevention. *Nat. Commun.* **9**, 4156 (2018).
10. Gunawardana, M. et al. Pharmacokinetics of long-acting tenofovir alafenamide (GS-7340) subdermal implant for HIV prophylaxis. *Antimicrob. Agents Chemother.* **59**, 3913–3919 (2015).
11. Flexner, C. Antiretroviral implants for treatment and prevention of HIV infection. *Curr. Opin. HIV AIDS* **13**, 374–380 (2018).
12. Barrett, S. E. et al. Extended-duration MK-8591-eluting implant as a candidate for HIV treatment and prevention. *Antimicrob. Agents Chemother.* **62**, e01058-18 (2018).
13. Markowitz, M. et al. Safety and tolerability of long-acting cabotegravir injections in HIV-uninfected men (ECLAIR): a multicentre, double-blind, randomised, placebo-controlled, phase 2a trial. *Lancet HIV* **4**, e331–e340 (2017).

14. Zhou, T. et al. Creation of a nanoformulated cabotegravir prodrug with improved antiretroviral profiles. *Biomaterials* **151**, 53–65 (2018).
15. Dash, P. K. et al. Sequential LASER ART and CRISPR treatments eliminate HIV-1 in a subset of infected humanized mice. *Nat. Commun.* **10**, 2753 (2019).
16. Hilaire, J. R. et al. Creation of a long-acting rilpivirine prodrug nanoformulation. *J. Control. Release* **311–312**, 201–211 (2019).
17. Sillman, B. et al. Creation of a long-acting nanoformulated dolutegravir. *Nat. Commun.* **9**, 443 (2018).
18. Smith, N. et al. A long acting nanoformulated lamivudine ProTide. *Biomaterials* **223**, 119476 (2019).
19. Soni, D. et al. Synthesis of a long acting nanoformulated emtricitabine ProTide. *Biomaterials* **222**, 119441 (2019).
20. Huttunen, K. M., Raunio, H. & Rautio, J. Prodrugs—from serendipity to rational design. *Pharm. Rev.* **63**, 750–771 (2011).
21. Rautio, J. et al. Prodrugs: design and clinical applications. *Nat. Rev. Drug Discov.* **7**, 255–270 (2008).
22. Bahar, F. G., Ohura, K., Ogihara, T. & Imai, T. Species difference of esterase expression and hydrolase activity in plasma. *J. Pharm. Sci.* **101**, 3979–3988 (2012).
23. Malamatari, M., Taylor, K. M. G., Malamataris, S., Douroumis, D. & Kachrimanis, K. Pharmaceutical nanocrystals: production by wet milling and applications. *Drug Discov. Today* **23**, 534–547 (2018).
24. Zhou, T. et al. Optimizing the preparation and stability of decorated antiretroviral drug nanocrystals. *Nanomedicine (Lond.)* **13**, 871–885 (2018).
25. Darville, N. et al. Intramuscular administration of paliperidone palmitate extended-release injectable microsuspension induces a subclinical inflammatory reaction modulating the pharmacokinetics in rats. *J. Pharm. Sci.* **103**, 2072–2087 (2014).
26. Kadiu, I., Nowacek, A., McMillan, J. & Gendelman, H. E. Macrophage endocytic trafficking of antiretroviral nanoparticles. *Nanomedicine (Lond.)* **6**, 975–994 (2011).
27. Nowacek, A., Kadiu, I., McMillan, J. & Gendelman, H. E. Immunoisolation of nanoparticles containing endocytic vesicles for drug quantitation. *Methods Mol. Biol.* **991**, 41–46 (2013).
28. McMillan, J. et al. Pharmacokinetics of a long-acting nanoformulated dolutegravir prodrug in rhesus macaques. *Antimicrob. Agents Chemother.* **62**, e01316-17 (2017).
29. Rohani, S., Horne, S. & Murthy, K. Control of product quality in batch crystallization of pharmaceuticals and fine chemicals. Part 1: design of the crystallization process and the effect of solvent. *Org. Process Res. Dev.* **9**, 858–872 (2005).
30. Nair, A. B. & Jacob, S. A simple practice guide for dose conversion between animals and human. *J. Basic Clin. Pharm.* **7**, 27–31 (2016).
31. Kerrigan, D. et al. Experiences with long acting injectable ART: a qualitative study among PLHIV participating in a Phase II study of cabotegravir + rilpivirine (LATTE-2) in the United States and Spain. *PLoS ONE* **13**, e0190487 (2018).
32. Osterberg, L. & Blaschke, T. Adherence to medication. *N. Engl. J. Med.* **353**, 487–497 (2005).
33. Shubber, Z. et al. Patient-reported barriers to adherence to antiretroviral therapy: a systematic review and meta-analysis. *PLoS Med.* **13**, e1002183 (2016).
34. Edagwa, B., McMillan, J., Sillman, B. & Gendelman, H. E. Long-acting slow effective release antiretroviral therapy. *Expert Opin. Drug Deliv.* **14**, 1281–1291 (2017).
35. Trezza, C., Ford, S. L., Spreen, W., Pan, R. & Piscitelli, S. Formulation and pharmacology of long-acting cabotegravir. *Curr. Opin. HIV AIDS* **10**, 239–245 (2015).
36. Wang, D. et al. Human carboxylesterases: a comprehensive review. *Acta Pharma. Sin. B* **8**, 699–712 (2018).
37. McPherson, T. D., Sobieszczyk, M. E. & Markowitz, M. Cabotegravir in the treatment and prevention of human immunodeficiency virus-1. *Expert Opin. Investig. Drugs* **27**, 413–420 (2018).
38. Stellbrink, H. J. & Hoffmann, C. Cabotegravir: its potential for antiretroviral therapy and preexposure prophylaxis. *Curr. Opin. HIV AIDS* **13**, 334–340 (2018).
39. Rautio, J., Meanwell, N. A., Di, L. & Hageman, M. J. The expanding role of prodrugs in contemporary drug design and development. *Nat. Rev. Drug Discov.* **17**, 559–587 (2018).
40. Landovitz, R. J. et al. Safety, tolerability, and pharmacokinetics of long-acting injectable cabotegravir in low-risk HIV-uninfected individuals: HPTN 077, a phase 2a randomized controlled trial. *PLoS Med.* **15**, e1002690 (2018).
41. Murray, M. I. et al. Satisfaction and acceptability of cabotegravir long-acting injectable suspension for prevention of HIV: patient perspectives from the ECLAIR trial. *HIV Clin. Trials* **19**, 129–138 (2018).
42. Penrose, K. J. et al. Selection of rilpivirine-resistant HIV-1 in a seroconverter from the SSAT 040 trial who received the 300-mg dose of long-acting rilpivirine (TMC278LA). *J. Infect. Dis.* **213**, 1013–1017 (2016).
43. Bollinger R. C. et al. Addressing the global burden of hepatitis B virus while developing long-acting injectables for the prevention and treatment of HIV. *Lancet HIV* https://doi.org/10.1016/S2352-3018(19)30342-X (2019).
44. Ford, S. L. et al. Effect of rifampin on the single-dose pharmacokinetics of oral cabotegravir in healthy subjects. *Antimicrob. Agents Chemother.* **61**, e00487-17 (2017).
45. Rajoli, R. K. R. et al. Predicting drug–drug interactions between rifampicin and long-acting cabotegravir and rilpivirine using physiologically based pharmacokinetic modeling. *J. Infect. Dis.* **219**, 1735–1742 (2019).
46. *Experimental HIV Vaccine Regimen Ineffective In preventing HIV* (National Institute of Allergy and Infectious Diseases, 2020); https://www.nih.gov/news-events/news-releases/experimental-hiv-vaccine-regimen-ineffective-preventing-hiv.
47. Benitez-Gutierrez, L. et al. Treatment and prevention of HIV infection with long-acting antiretrovirals. *Expert Rev. Clin. Pharm.* **11**, 507–517 (2018).
48. de Mendoza, C. & Soriano, V. Tough requirements for new antiretroviral drugs. *Lancet HIV* **7**, e150–e151 (2020).
49. Smith, R. A. et al. In vitro antiviral activity of cabotegravir against HIV-2. *Antimicrob. Agents Chemother.* **62**, e01299-18 (2018).

Methods

Reagents. CAB was purchased from BOC Sciences. Pyridine, DMF, DIEA, myristoyl chloride, stearoyl chloride, behenic acid, pluronic F127 (P407), polyethylene glycol 3350, ciprofloxacin, MTT, dimethyl sulfoxide, paraformaldehyde (PFA) and 3,3′-diaminobenzidine were purchased from Sigma-Aldrich. Diethyl ether, ethyl acetate, hexanes, ACN, methanol (MeOH), mass-spectrometry-grade water, cell-culture-grade water (endotoxin free), gentamicin, potassium phosphate monobasic, bovine serum albumin, Triton X-100 and TRIzol reagent were purchased from Fisher Scientific. Monoclonal mouse anti-human HIV-1 p24 (clone Kal-1) and polymer-based horseradish-peroxidase-conjugated anti-mouse EnVision+ secondary were purchased from Dako. Heat-inactivated pooled human serum was purchased from Innovative Biologics. DDMEM was purchased from Corning Life Sciences.

Synthesis and characterization of CAB prodrugs. A series of three prodrugs were synthesized by the esterification of the hydroxyl group on CAB to yield lipophilic prodrugs with 14, 18 and 22 carbon chains (MCAB, M2CAB and M3CAB, respectively). Specifically, CAB was dried from anhydrous pyridine and then suspended in anhydrous DMF. The mixture was cooled to 0 °C under argon. DIEA (2 equiv.) was used to deprotonate the hydroxyl group of CAB and then reacted with 2 equiv. myristoyl and stearoyl chloride for 24 h to obtain MCAB and M2CAB, respectively. M3CAB was synthesized in a two-step process. First, behenyl chloride was synthesized by reacting 1 equiv. behenic acid with 4 equiv. thionyl chloride in anhydrous chloroform. The formed acyl chloride was then covalently linked to CAB in the second step to form the M3CAB prodrug. All the resultant prodrugs were purified by silica gel column chromatography using an eluent of a 4:1 then 9:1 mixture of ethyl acetate and hexanes. The desired compound fractions from the columns were dried on a rotary evaporator, precipitated from diethyl ether to obtain white powders, which were further dried under a high vacuum to give average chemical yields of 85–95%. The successful synthesis of prodrugs was confirmed by ^{1}H and ^{13}C NMR spectroscopy using a Bruker Avance-III HD operating at 500 MHz and a magnetic field strength of 11.7 T. FTIR was performed on an IR-Prestige 21 (Shimadzu). Comparative crystallographic analyses of CAB and the prodrugs by XRD were carried out in the 2θ range of 2–70° at a rate of 1° s^{-1} using a PANalytical Empyrean diffractometer (PANalytical Inc.) with Cu Kα radiation (1.5418 Å) at a 40 kV, 45 mA setting. The molecular mass was determined by direct infusion into a triple quadrupole mass spectrometer.

Ultraperformance liquid chromatography–ultraviolet/visible quantification of CAB, MCAB, M2CAB and M3CAB. A Waters ACQUITY ultraperformance liquid chromatography H-Class system with a tunable ultraviolet detector and Empower 3 software was used to measure the drug concentrations. CAB, MCAB, M2CAB and M3CAB samples were separated on a Phenomenex Kinetex 5 µm C18 column (150 × 4.6 mm). CAB was detected at 254 nm using an isocratic elution with a mobile phase that consisted of 65% 50 mM potassium phosphate monobasic (pH 3.2) and 35% ACN and with a flow rate of 1.0 ml min^{-1}. MCAB, M2CAB and M3CAB were detected at 230 nm using a gradient elution that started with a mobile phase consisting of 90% ACN/10% water to 95% ACN/5% water and finally to 98% ACN/2% water at a flow rate of 1.0 ml min^{-1}. The drug content was determined relative to the peak areas of drug standards (0.05–50 µg ml^{-1}) in MeOH.

Solubility. The log P, aqueous solubility and 1-octanol solubility of CAB, MCAB, M2CAB and M3CAB were determined by adding the drug to a mixture of water and 1-octanol at room temperature and then mixing for 48 h. Samples were centrifuged at 20,000g for 10 min to an insoluble pellet drug. Aqueous supernatants were frozen, lyophilized and then resuspended in MeOH. 1-octanol supernatants were prepared for analysis by dilution in MeOH and samples analysed for drug content by UPLC.

Plasma prodrug cleavage kinetics. The hydrolysis kinetics of MCAB, M2CAB and M3CAB and release of the active drug were determined in plasma of different species (mouse, rat, rabbit, monkey, dog and human). MCAB, M2CAB and M3CAB (1 µM) were incubated in 100 µl of plasma at 37 °C. At specified time points, 1 ml of MeOH buffer (0.1% formic acid, 25 mM ammonium formate) was added to each sample and vortexed for 3 min to stop the reaction. For the 0-min time point, 100 µl of ice cold plasma was spiked with 1 µM of each prodrug, and 1 ml of ice-cold MeOH buffer was added immediately. After the addition of MeOH, samples were centrifuged at 15,000g for 10 min and the supernatants were analysed for drug content by UPLC–MS/MS (Waters Xevo TQ-XS).

Nanoparticle synthesis and characterization. NCAB and the prodrugs NMCAB, NM2CAB and NM3CAB were manufactured by high-pressure homogenization using the surfactant P407. Briefly, each solid drug/prodrug was dispersed in a P407 solution in endotoxin-free water and allowed to form a presuspension. The drug/prodrug to surfactant ratio was maintained at 10:1 (w/w), and the suspension concentration was in the range 2–20% w/v for the drug/prodrug and 0.2–2% w/v for P407. The presuspension was homogenized on an Avestin EmulsiFlex-C3 high-pressure homogenizer at 1.24 × 10^8 Pa until the desired particle size was achieved. Nanoparticles were characterized for particle size, PDI and zeta potential

by dynamic light scattering using a Malvern Zetasizer Nano-ZS. The stabilities of the nanoformulations were monitored at 4 °C, room temperature and 37 °C for 3 months. The drug/prodrug concentration in each nanoformulation was determined by dissolving the nanoformulation in MeOH (1,000–10,000-fold dilution) which was then analysed by UPLC–ultraviolet/visible (UV/vis) spectroscopy. The encapsulation efficiency was calculated using the equation: encapsulation efficiency (%) = (weight of drug in formulation/initial weight of drug added) × 100. Drug loading was calculated using the equation: drug loading (%) = (weight of drug in formulation/weight of lyophilized formulation) × 100. For quantitation of the uncoated drug in nanosuspensions, homogenized drug formulations (NCAB and NM2CAB) were centrifuged at 20,000g for 10 min to pellet the nanoformulated drug. Supernatants were frozen, lyophilized and subsequently resuspended in MeOH for analyses. Collected samples were analysed for drug content by UPLC–UV/vis spectroscopy as previously described. Nanoparticle morphologies were assessed by SEM. Nanoparticles were fixed in a solution of 2% glutaraldehyde and 2% PFA in 0.1 M Sorenson's phosphate buffer (pH 7.2) at 4 °C for 24 h, and processed for imaging. Nanosuspensions were air-dried onto a glass coverslip mounted on an SEM sample stub and sputter coated with approximately 50 nm of a gold/palladium alloy. Samples were assayed using a FEI Quanta 200 scanning electron microscope operated at 5.0 kV (ref. [17]).

Human MDMs. Human monocytes were obtained by leukapheresis from HIV-1/2 and hepatitis B seronegative donors and purified by counter-current centrifugal elutriation. Monocytes were cultured in DMEM that contained 4.5 g l^{-1} glucose, L-glutamine, and sodium pyruvate supplemented with 10% heat-inactivated human serum, 50 µg ml^{-1} gentamicin and 10 µg ml^{-1} ciprofloxacin. Cells were maintained at 37 °C in a 5% CO$_2$ incubator. Recombinant human macrophage colony stimulating factor (1,000 U ml^{-1}) was added to the culture media for the first 7 days to facilitate monocyte differentiation into MDMs. Half-culture media were replaced with fresh media every other day. After differentiation, MDMs were used for the in vitro assays.

Cytotoxicity. The cell viability after treatment with nanoparticles was evaluated using the MTT assay. Human MDMs plated in 96-well plates at a density of 0.08 × 10^6 cells per well were treated with 10, 25, 50, 100, 200 or 400 µM NCAB, NMCAB, NM2CAB or NM3CAB for 24 h. Untreated cells were used as controls. For each group, quadruplicate samples were used. The cells were washed with phosphate buffered saline (PBS) and incubated with 100 µl per well of MTT solution (5 mg ml^{-1}) for 45 min at 37 °C. After incubation, the MTT solution was removed, and the cells were washed with PBS. Next, dimethyl sulfoxide (200 µl) was added to each well, and the absorbance was measured at 490 nm on a Molecular Devices SpectraMax M3 plate reader with SoftMax Pro 6.2 software. Absorbance was compared with that of control cells to determine the cytotoxicity.

Drug particle uptake, retention and release. Human MDMs were used for in vitro assessments. MDM uptake and retention studies were performed in flat-bottom, 12-well plates at a density of 1 × 10^6 cells per well, with each treatment completed in triplicate. For cellular uptake studies, MDMs were treated with 100 µM NCAB, NMCAB, NM2CAB or NM3CAB. At 2, 4, 8 and 24 h after treatment, the medium was removed; MDMs were washed twice with PBS then scraped into 1 ml of PBS and counted (Invitrogen Countess Automated Cell Counter). Cells were pelleted by centrifugation at 950g for 8 min at 4 °C. Cell pellets were resuspended in 200 µl of HPLC-grade MeOH and sonicated using a probe sonicator to release the intracellular drug and prodrug. For the retention studies, MDMs were treated with 100 µM NCAB, NMCAB, NM2CAB or NM3CAB for 8 h, and then washed twice with PBS. Fresh culture medium without the drug was added, and a half-media volume was replaced every other day. MDMs were collected at days 1, 5, 10, 15, 20, 25 and 30, and then processed as described for the uptake studies to assay the intracellular drug and prodrug concentrations. For both studies, the resultant lysates were centrifuged at 20,000g for 10 min at 4 °C to separate cell debris from the drug-containing supernatant. Samples were analysed for drug and prodrug content by UPLC–UV/vis spectroscopy. For release studies, culture media at time points similar to those in the retention study were collected to quantitate the drug and prodrug released by the MDMs. The culture medium (400 µl) was mixed with MeOH (1 ml) to precipitate proteins and then centrifuged at 17,000g for 10 min at 4 °C to pellet the non-soluble precipitate. The supernatant was transferred to new tubes and dried using a SpeedVac (ThermoFisher Scientific). The dried contents were resuspended in MeOH and analysed by UPLC–UV/vis spectroscopy.

Intracellular particle distribution. MDMs were treated with 100 µM NCAB, NMCAB, NM2CAB or NM3CAB for 8 h and then washed twice with PBS. Fresh culture medium without the drug was added, and a half-media volume was replaced every other day. MDMs were collected at days 0, 15 and 30 after treatment and analysed by TEM to image the intracellular nanoparticles. For day 0, the cells were collected immediately after the 8-h treatment. At stated time points, the cells were washed twice with PBS, scraped into PBS, pelleted at 950g for 8 min at room temperature and fixed in a solution of 2% glutaraldehyde and 2% PFA in 0.1 M Sorenson's phosphate buffer (pH 6.2). The fixed cell suspension was placed on a

formvar/silicon monoxide 200 mesh copper grid and allowed to settle for 2 min. Excess solution was wicked off, and the samples were allowed to dry. NanoVan vanadium negative stain was placed on the grid for 1 min, then wicked away and allowed to dry. Grids were examined on a FEI Tecnai G2 Spirit TWIN TEM operated at 80 kV. Images were acquired digitally with an AMT digital imaging system[17].

HIV-1 MDM infection. MDMs were plated in flat-bottom 24-well plates at a density of 0.8×10^6 cells per well. MDMs were treated with 100 μM NCAB, NMCAB, NM2CAB or NM3CAB for 8 h. After treatment, the cells were washed twice with PBS and cultured in fresh culture medium without drug with half-media replacement every other day. At 1, 5, 10, 15, 20, 25 and 30 days after the treatment, the cells were infected with HIV-1$_{ADA}$ at a multiplicity of infection of 0.1 infectious particles per cell for 16 h. After infection, MDMs were washed twice with PBS and replenished with fresh media without virus or drug. The cells were cultured for an additional 10 days with half-media replacement every other day and full medium replacement on the 8th day. The culture medium was collected on the 10th day after infection to measure the HIV-1 RT activity. The extent of infection was determined as the percent of RT activity relative to the infected untreated MDM. Cells were fixed in 2% PFA at each time point, and expression of the HIV-1 p24 antigen was determined by immunocytochemistry.

EC$_{50}$ test. MDMs were plated in flat-bottom 96-well plates (0.08×10^6 cells per well). Cells were treated with a range of drug concentrations, 0.01–1,000 nM, of CAB, MCAB, M2CAB, M3CAB, NCAB, NMCAB, NM2CAB or NM3CAB for 1 h prior to infection with HIV-1$_{ADA}$ (multiplicity of infection of 0.1) for 4 h. After 4 h of viral challenge, the cells were washed with PBS and given fresh media that contained the same concentrations of drug (0.01–1,000 nM). Cell supernatants were collected 10 days later and assayed for HIV-1 RT activity as described above.

PK, BD and drug–drug interaction studies. NSG mice (female, 6–8 weeks; Jackson Labs) were administered 45 mg per kg body weight CAB equivalents of NCAB, NMCAB, NM2CAB or NM3CAB by a single IM (caudal thigh muscle) injection at 40 μl per 25 g of mouse. After injection, blood samples were collected into heparinized tubes at day 1 postadministration and then weekly up to day 364 by cheek puncture (submandibular vein) using a 5 mm lancet (MEDIpoint, Inc.). The collected blood (25 μl) was immediately diluted into 1 ml of ACN for drug measurements. The remaining blood samples were centrifuged at 2,000g for 8 min for plasma collection and quantitation of the plasma drug contents. At days 14, 28, 42 and 364 after administration, animals were humanely euthanized, and spleen, lymph node, liver, lung, gut (duodenum/jejunum), kidney, brain, vaginal and rectal tissue were collected for the quantitation of CAB and prodrug concentrations. CAB, MCAB, M2CAB and M3CAB were quantitated in mouse plasma, blood and tissues by UPLC–MS/MS using a Waters ACQUITY H-class UPLC connected to a Xevo TQ-S micro mass spectrometer. All the solvents for sample processing and UPLC–MS/MS analysis were liquid chromatography–MS grade (Fisher). Details of the sample processing and quantitation methods are provided in Supplementary Methods. Non-compartmental PK analysis for plasma CAB in NSG mice was performed using Phoenix WinNonlin-8.0 software (Certara). Toxicity in the NSG mice was assessed by evaluating the serum chemistry profiles and histological examination. For the histological examination, 5-μm sections of paraffin-embedded tissues were stained with haematoxylin and eosin. Images were captured with a ×40 objective using a Nuance EX multispectral imaging system affixed to a Nikon Eclipse E800 microscope (Nikon Instruments). Histopathological assessments were conducted by a certified pathologist in accordance with the guidelines of the Society of Toxicologic Pathology. Serum chemistry profiles were determined using a VetScan comprehensive diagnostic profile disc and a VetScan VS-2 instrument (Abaxis Veterinary Diagnostics). The results for treated animals were compared with those from age-matched untreated control mice. The PK and BD of NM2CAB were also evaluated in BALB/cJ mice (male, 6–8 weeks; Jackson Labs). NCAB was used as a control. Mice were dosed with NM2CAB (45 mg per kg body weight CAB equivalents) by IM injection and were humanely euthanized at day 280 after treatment. Plasma and tissues were collected for drug and prodrug quantitation as described above for NSG mice. Drug–drug interactions between two prodrug nanoformulations, NM2CAB and NM3RPV, were evaluated in BALB/cJ mice (male, 6–8 weeks; Jackson Labs). Animals were treated IM with a single dose of NM2CAB alone (45 mg per kg body weight CAB equivalents), NM3RPV alone (45 mg per kg body weight RPV equivalents) or the co-administration of both prodrug nanoformulations (NM2CAB and NM3RPV, 45 mg per kg body weight drug equivalents for each). Plasma was collected up to day 49 for active drug (CAB and RPV) quantitation as described above for NSG mice.

PK and BD in RMs. For PK and BD studies in RMs, NM2CAB was prepared in the Nebraska Nanomedicine Production Plant using good laboratory practice protocols. The presuspension was prepared and homogenized as described above to form the final nanosuspension. Particle size, PDI and zeta potential were determined by dynamic light scattering (Malvern Zetasizer NanoZSP).

The M2CAB concentration in the nanosuspension was determined by UPLC–MS/MS (Waters Acquity Xevo TQ-S micro system) as described above. The endotoxin content was determined by the Lonza Limulus Amebocyte Lysate Pyrogent-500 test (Lonza) and was found to be less than 5 EU per kg body weight. Four male RMs (4.4–6.7 kg; PrimeGen) were anaesthetized with ketamine (10 mg per kg body weight); each was administered 45 mg per kg body weight CAB equivalents of NM2CAB and a lab-generated RPV prodrug nanoformulation[16] by IM injection (gluteus maximus, 0.5 ml per kg body weight). Blood samples were collected in potassium–EDTA coated tubes for complete blood counts, and plasma was isolated for metabolic profiles. Tissue biopsies of lymph nodes, adipose and rectal tissues were collected at day 204 after injection for drug quantitation. Drug and prodrug in plasma and tissues were quantitated by UPLC–MS/MS as described for the mouse samples.

Crystallization of M2CAB. Recrystallizations of 100 mg of M2CAB in 3.0 ml of ACN, methyltetrahydrofuran, CPME or toluene were carried out from the solubilized prodrug solution at 65 °C. The solutions were then gradually cooled to 20 °C and stirred for 16 h to form solid drug crystals that were consequently collected by filtration. Reproducibility of the recrystallization protocol was confirmed using 200 mg of M2CAB in ACN (4 ml). Chemical purity was measured by HPLC, and the melting points of the solid samples were measured using capillary tubes in a Stuart SMP10 melting point apparatus. The sample heating rate was 2 °C min^{-1}. The physical appearance of the solids after recrystallization from ACN and CPME was assessed by XRD.

Statistical analyses. Statistical analyses were conducted using GraphPad Prism 7.0 software. Data from in vitro studies were expressed as mean ± s.e.m. with a minimum of three biological replicates. Results from the in vivo studies were expressed as mean ± s.e.m. with a minimum of three biological replicates. For comparisons between two groups, t-test (two-tailed) with Welch's correction was used. A one-way ANOVA followed by Tukey's post hoc test was used to compare three or more groups. Statistical significances were denoted as *$P < 0.05$, **$P < 0.01$, ***$P < 0.001$ and ****$P < 0.0001$. Linear regression models were used to examine the association between in vitro data and PK data.

Study approvals. All the animal studies were approved by the University of Nebraska Medical Center Institutional Animal Care and Use Committee in accordance with the standards incorporated in the *Guide for the Care and Use of Laboratory Animals*[50]. Human monocytes were isolated by leukapheresis from HIV-1/2 and hepatitis B seronegative donors according to an approved University of Nebraska Medical Center Institutional Review Board exempt protocol.

Reporting summary. Further information on research design is available in the Nature Research Reporting Summary linked to this article.

Data availability
The data supporting the study's findings are available within the article and its supplementary files or from the corresponding authors upon request. All the relevant data used to generate Figs. 4a,c,k, 5a–i and 6a–c are included as Source Data.

References
50. Committee for the Update of the Guide for the Care and Use of Laboratory Animals *Guide for the Care and Use of Laboratory Animals* 8th edn (National Academies, 2011).

Acknowledgements

Author contributions

T.A.K. synthesized the prodrugs, performed the formulation characterization and cell-based laboratory experiments and interpreted the data, prepared the figure, and co-wrote the manuscript. A.N.B. designed and carried out the laboratory and rodent experiments, analysed and interpreted the data, supervised the project, prepared the figures and tables, and co-wrote and edited the manuscript. B.S., B.L.D.S., M.S.W., N.G., J.R.H. and S.S. performed the laboratory, physicochemical and/or rodent experiments. A.S. prepared NM2CAB in the Nebraska Nanomedicine Production Plant using good laboratory practice protocols. B.G.L., B.M.M. and H.S.F. performed and analysed the data from the non-human primate experiments. P.L.D., T.-Y.Y. and G.M. designed and executed the prodrug recrystallization, scale up and formulation manufacture experiments. Y.A. performed the data acquisition and interpretation. J.M.M. designed, supervised and analysed the mass spectrometry data. R.L.M. and J.M. performed statistical evaluations and data analyses. B.J.E. was responsible for the project conception, study and prodrug design, chemical drug synthesis and nanoformulation schemes, provided supervision, data analyses and interpretation, manuscript editing and funding acquisitions. H.E.G. was responsible for the project conception and study integration, integrated each of the study arms, supervised experimental design and data interpretation, co-wrote and edited the manuscript and provided funding acquisitions. All the authors critically evaluated the manuscript prior to submission.

Competing interests

B.J.E. and H.E.G. are named inventors on patents that cover the medicinal and polymer chemistry technologies employed in this article that encompass the synthesis of long-acting cabotegravir prodrugs and formulation manufacturing. H.E.G. is the Interim Director of the Nebraska Nanomedicine Production Plant, a good manufacturing programme facility. The authors declare that this work was produced solely by the authors and that no other individuals or entities influenced any aspects of the work including, but not limited to, the study conception and design, data acquisition, analyses and interpretation, and writing of the manuscript. No other entities provided funds for the work. The authors further declare that they have received no financial compensation from any other third parties for any aspects of the published work. The remaining authors declare no competing interests.

Additional information

Supplementary information is available for this paper at https://doi.org/10.1038/s41563-020-0674-z.

Correspondence and requests for materials should be addressed to B.J.E. or H.E.G.

Reprints and permissions information is available at www.nature.com/reprints.

nature research

Corresponding author(s):	Drs. Howard E. Gendelman and Benson J. Edagwa
Last updated by author(s):	Mar 17, 2020

Reporting Summary

Nature Research wishes to improve the reproducibility of the work that we publish. This form provides structure for consistency and transparency in reporting. For further information on Nature Research policies, see Authors & Referees and the Editorial Policy Checklist.

Statistics

For all statistical analyses, confirm that the following items are present in the figure legend, table legend, main text, or Methods section.

n/a	Confirmed	
☐	☒	The exact sample size (n) for each experimental group/condition, given as a discrete number and unit of measurement
☐	☒	A statement on whether measurements were taken from distinct samples or whether the same sample was measured repeatedly
☐	☒	The statistical test(s) used AND whether they are one- or two-sided *Only common tests should be described solely by name; describe more complex techniques in the Methods section.*
☒	☐	A description of all covariates tested
☐	☒	A description of any assumptions or corrections, such as tests of normality and adjustment for multiple comparisons
☐	☒	A full description of the statistical parameters including central tendency (e.g. means) or other basic estimates (e.g. regression coefficient) AND variation (e.g. standard deviation) or associated estimates of uncertainty (e.g. confidence intervals)
☐	☒	For null hypothesis testing, the test statistic (e.g. F, t, r) with confidence intervals, effect sizes, degrees of freedom and P value noted *Give P values as exact values whenever suitable.*
☒	☐	For Bayesian analysis, information on the choice of priors and Markov chain Monte Carlo settings
☒	☐	For hierarchical and complex designs, identification of the appropriate level for tests and full reporting of outcomes
☒	☐	Estimates of effect sizes (e.g. Cohen's d, Pearson's r), indicating how they were calculated

Our web collection on statistics for biologists contains articles on many of the points above.

Software and code

Policy information about availability of computer code

Data collection	Empower 3 software (Milford, MA) and SoftMax Pro 6.2 software (Sunnyvale, CA)
Data analysis	Statistical analyses were conducted using GraphPad Prism 7.0 software (La Jolla, CA). Non-compartmental PK analysis for plasma drug levels was performed using Phoenix WinNonlin-8.0 software (Certara, Princeton, NJ).

For manuscripts utilizing custom algorithms or software that are central to the research but not yet described in published literature, software must be made available to editors/reviewers. We strongly encourage code deposition in a community repository (e.g. GitHub). See the Nature Research guidelines for submitting code & software for further information.

Data

Policy information about availability of data

All manuscripts must include a data availability statement. This statement should provide the following information, where applicable:
- Accession codes, unique identifiers, or web links for publicly available datasets
- A list of figures that have associated raw data
- A description of any restrictions on data availability

All data generated or analyzed during this study are included in this published article (and its supplementary information files).

Field-specific reporting

Please select the one below that is the best fit for your research. If you are not sure, read the appropriate sections before making your selection.

☒ Life sciences   ☐ Behavioural & social sciences   ☐ Ecological, evolutionary & environmental sciences

Life sciences study design

All studies must disclose on these points even when the disclosure is negative.

Sample size	No statistical method was used to predetermine the sample sizes which were based on work in similarly published research. Sample size chosen were sufficient to determine significance in all assays, with reproducible statistical significance difference between experimental conditions. For animal studies, sample sizes were predetermined in order to provide statistical power while also meeting cost and ethical criteria for animal use.
Data exclusions	Exclusion criteria was predetermined. Extreme outliers beyond the 99% confidence interval of the mean and 3-fold greater than the SEM were excluded.
Replication	All attempts to reproduce the experimental findings were successful. For chemical synthesis and characterization, experiments were repeated independently minimum five times with similar results. For in vitro cellular assays, experiments were repeated independently minimum three times with similar results. For animal studies, results of one year long study were validated in different strains of mice and species (mice and rhesus macaques)
Randomization	For all studies, samples/cells/animals were randomly allocated into experimental groups at the beginning of each study.
Blinding	Investigators were not blinded in conducting experiments or sample collection relying on unbiased approach. However, for drug level analysis in cells and animal samples, investigators were blinded during data collection. For pathological evaluation of histology sections of tissues, pathologist was blinded.

Reporting for specific materials, systems and methods

We require information from authors about some types of materials, experimental systems and methods used in many studies. Here, indicate whether each material, system or method listed is relevant to your study. If you are not sure if a list item applies to your research, read the appropriate section before selecting a response.

Materials & experimental systems

n/a	Involved in the study
☐	☒ Antibodies
☒	☐ Eukaryotic cell lines
☒	☐ Palaeontology
☐	☒ Animals and other organisms
☒	☐ Human research participants
☒	☐ Clinical data

Methods

n/a	Involved in the study
☒	☐ ChIP-seq
☒	☐ Flow cytometry
☒	☐ MRI-based neuroimaging

Antibodies

Antibodies used	Monoclonal mouse anti-human HIV-1p24 [Catlog number. M0857; Clone. Kal-1; Agilent (Original Manufacturer: Dako. Now part of Agilent.), Carpenteria, CA, USA)]; Nkwe DO et al. 2016, PMID 27338237
Validation	HIV-1p24 antibody provides excellent specificity, high lot to lot consistency, and certified manufacturing facilities guarantee full quality control (per company website). Antibody was validated and reported in previous publications [Nkwe DO et al. 2016, Gnanadhas DP. et al. 2017; Sillaman, B. et al. 2018; Hilaire JR. et al. 2019; Soni D. et al 2019; Smith N. et al 2019].

Animals and other organisms

Policy information about studies involving animals; ARRIVE guidelines recommended for reporting animal research

Laboratory animals	A) Mice: 1) NSG, Female, 6-8 weeks age and 2) BALB/cJ, Male, 6-8 weeks age; B) Rhesus Macaques, Male, 5-6 years age
Wild animals	The study did not involve wild animals.
Field-collected samples	The study did not involve samples collected from the field.
Ethics oversight	All experimental protocols involving the use of laboratory animals were approved by the UNMC Institutional Animal Care and Use Committee (IACUC) ensuring the ethical care and use of laboratory animals in experimental research. All animal studies were performed in compliance with UNMC institutional policies and NIH guidelines for laboratory animal housing and care. Human monocytes were isolated by leukapheresis from HIV-1/2 and hepatitis B seronegative donors according to an approved UNMC Institutional Review Board exempt protocol.

Note that full information on the approval of the study protocol must also be provided in the manuscript.